(19,735 characters)

Mitotic ER exit site dissociation is mediated by TANGO1 phosphorylation with CK1.

Miharu Maeda, Yukie Komatsu and Kota Saito

Department of Biological Informatics and Experimental Therapeutics, Graduate School of Medicine, Akita University 1-1-1, Hondo, Akita, 010-8543, Japan

Running title: CK1 phosphorylates TANGO1 for mitotic ERES break.

Correspondence to Kota Saito (ksaito@med.akita-u.ac.jp)

Summary: The mechanisms of ER exit block during mitosis is not well-understood. Maeda et al. report that casein kinase 1 phosphorylates TANGO1 to abrogate the interaction with Sec16, causing ER exit site dissociation during mitosis.

Abstract

Golgi fragmentation and ER exit site dissociation are considered as the leading causes of mitotic block of secretion from the ER. Although the mechanisms of Golgi fragmentation have been extensively characterized, ER exit block early in mitosis is not well-understood. We previously found that TANGO1 organizes ER exit sites by directly interacting with Sec16. Here, we showed that TANGO1 is phosphorylated by casein kinase 1 (CK1) during mitosis. Interestingly, the interaction with Sec16 was abrogated by phosphorylation of TANGO1, leading to dissociation of the ER exit sites. Moreover, a TANGO1 mutant deficient in phosphorylation inhibited the mitotic dissociation of ER exit sites. In contrast, a TANGO1 mutant mimicking CK1-mediated phosphorylation dissociated ER exit sites in interphase cells. This is the first report demonstrating the mechanisms of ER exit site dissociation during mitosis.

Introduction

ER to Golgi traffic is blocked during mitosis (Kreiner and Moore, 1990; Warren et al., 1983). Mitotic Golgi are fragmented into haze, and it remains controversial whether the Golgi membrane fuses with the ER or remain segregated during mitosis (Pecot and Malhotra, 2004; Sengupta et al., 2015; Villeneuve et al., 2017; Zaal et al., 1999). The ER exit site, a specific domain on the ER for vesicle budding, dissociates during mitosis (Farmaki et al., 1999), but the mechanisms remain unclear. In interphase cells, mammalian ER exit sites consist of 2–6 cytoplasmic coat protein II (COPII)-coated pits according to electron microscopic analysis (Bannykh et al., 1996; Zeuschner et al., 2006). Although COPII-vesicle formation at ER exit sites has been extensively characterized, the biogenesis of ER exit sites is poorly understood. Sec16, a peripheral membrane protein localized at ER exit sites, is thought to be an organizer of these sites (Miller and Schekman, 2013). However, it must first be recruited to ER membranes to perform its functions. TANGO1(L) was identified as cargo receptor for large cargoes including collagens and chylomicrons (Saito et al., 2009; Santos et al., 2016). Recent analysis suggested that TANGO1L, in cooperation with its alternative spliced isoform, TANGO1S, organize the ER exit site by interacting and recruiting Sec16 to the ER exit sites (Maeda et al., 2017; Maeda et al., 2016). Thus, Sec16 and TANGO1 are key organizers of ER exit sites (Saito et al., 2017). Here, we identified casein kinase 1 (CK1) as a regulator of ER exit sites. We found that TANGO1 phosphorylation by CK1 reduces its interaction with Sec16 to disorganize ER exit sites during mitosis.

Results and discussion

CK1 regulates ER exit site organization

Although previous reports suggested that CK1δ is involved in COPII vesicle budding from the ER (Lord et al., 2011), the mechanisms were unclear. First, we expressed CK1α and CK1δ and evaluated their effects on ER exit site organization. CK1α expression did not affect the localization of Sec16 and Sec31 (Fig. 1A upper panel). In contrast, CK1δ expression resulted in dissociation of Sec16 and Sec31, as observed in cells depleted of TANGO1L and TANGO1S (Fig. 1A middle panel) (Maeda et al., 2017). The kinase inactive form of CK1δ, K38R, did not induce dissociation, suggesting that kinase activity is required for this process (Fig. 1A, bottom panel). Quantitative analysis showed that the colocalization efficiency between Sec16 and Sec31 was significantly reduced by expression of CK1δ but not by CK1α or CK1δ K38R (Fig. 1B). CK1δ expression did not alter the expression of other proteins tested including TANGO1 (Fig. 1C). Because the function of CK1δ considerably overlaps with CK1ε (Schittek and Sinnberg, 2014; Venerando et al., 2014), we next examined the organization of ER exit sites upon depletion of CK1δ and CK1ε. As shown in Fig. 1D, following depletion of CK1 δ and CK1ε, ER exit sites stained by Sec16, Sec23, and Sec31 were enlarged. Quantitative analysis revealed that the numbers of small and large ER exit sites were decreased and increased, respectively, following CK1 depletion (Fig. 1E), without affecting the expression of other proteins (Fig. 1F). Next, we used IC261, an ATP-competitive specific inhibitor for CK1δ and CK1ε (Mashhoon et al., 2000). Interestingly, cells treated with the inhibitor showed a similar phenotype as CK1-depleted cells (Fig. 1G and H). These results suggest that CK1δ and CK1ε are involved in organizing ER exit sites through their kinase activities. Because Sec23 has been identified as a substrate for CK1 (Lord et al., 2011), we predicted that CK1-mediated Sec23 phosphorylation regulates the organization of ER exit sites. In this case, Sec23 depletion would eliminate the effect of IC261-mediated enlargement of ER exit sites. We depleted Sec23 from HeLa cells and examined the size of ER exit sites. As shown in Fig. 1I and J, enlarged ER exit sites were still observed following IC261 treatment, even in Sec23-depleted cells. Thus, it is unlikely that CK1-mediated regulation of ER exit site size is mediated by Sec23 phosphorylation.

CK1 interaction reduces the binding affinity of Sec16 to TANGO1

To further investigate the effect of CK1 on ER exit site organization, we examined whether CK1 interacts with other proteins at ER exit sites. As shown in Fig. 2A, we found that CK1δ interacts with Sec16 (Fig. 2A, lanes 1 and 2). The kinase activity of CK1δ did not affect this interaction (Fig. 2A, lanes 3 and 4). To determine the interaction domain on Sec16, we examined the interaction of deletion constructs of Sec16 with CK1 (Fig. 2B). Sec16 (1101–1600) and Sec16 (1601–1890) efficiently interacted with CK1δ (Fig. 2C). When Sec16 was truncated into the TANGO1-interacting region (1101–1400), the interaction was reduced but not eliminated (Fig. 2C) (Maeda et al., 2017). These results suggest that Sec16 possesses multiple CK1-interacting regions which can be mapped to Sec16 (1101–1890). In contrast, TANGO1S failed to interact with CK1 (Fig. 2D). We previously showed that the interaction between TANGO1 and Sec16 is vital for proper ER exit site organization (Maeda et al., 2017). Thus, we next examined whether CK1 regulates ER exit site organization via TANGO1/Sec16. As expected, Sec16 interacted with both TANGO1S and CK1δ; however, the interaction between TANGO1 and Sec16 was markedly reduced when CK1δ was added (Fig. 2E). These results indicate that CK1 organizes ER exit sites by changing the interaction properties between TANGO1 and Sec16.

CK1-mediated TANGO1 phosphorylation dissociates ER exit sites

The above results suggest that the kinase activity of CK1 is important for ER exit site organization. Thus, we searched for possible phosphorylation sites within TANGO1 and Sec16 using the PhosphositePlus and NetPhos databases (Blom et al., 1999; Hornbeck et al., 2015). We found phosphorylation hotspots within TANGO1 just upstream of the proline-rich domain (PRD) and named these sites as phosphorylation predicted sequences (PPS) (Fig. 3A). PPS alignment indicated that this region is well-conserved among species (Fig. S1A). Next, we mutated serine or threonine to alanine in the PPS (SA mutant) and evaluated whether this region is phosphorylated via CK1 in an *in vitro* kinase assay. We used CK1 without the C-terminal regulatory domain for hyperactivation (Graves and Roach, 1995). Recombinant TANGO1 PPS+PRD or the corresponding SA mutant were incubated either with wild-type or kinase-dead CK1δ in the presence of [γ-^{32}P] ATP (Fig. S1B). As shown in Fig. 3B, wild-type CK1δ efficiently phosphorylated TANGO1 PPS+PRD but failed to phosphorylate the SA mutant, strongly suggesting that the TANGO1 PPS is phosphorylated by CK1δ. The inefficient phosphorylation by

kinase-dead CK1 validated the specificity of this effect. Next, we prepared TANGO1S with the phosphorylation mimic (TANGO1S (SE)-HA) or inefficient mutations (TANGO1S (SA)-HA) and examined their interactions with Sec16. Coimmunoprecipitation analysis revealed that SE mutants reduced the binding to Sec16, whereas SA mutants enhanced the binding to Sec16 compared to wild-type TANGO1S (Fig. 3C). These data indicate that phosphorylation of TANGO1 by CK1 reduced the interaction with Sec16. Indeed, the interaction between TANGO1 and Sec16 was not susceptible to CK1δ when the TANGO1 SA mutant was used rather than the wild-type protein (Compare Fig. 2E and Fig. 3D). Next, we examined whether TANGO1 mutants affect the organization of ER exit sites. We previously showed that Sec16 and Sec31 dissociates upon TANGO1 depletion, which cannot be rescued by TANGO1 lacking the Sec16-interacting region (Maeda et al., 2017). We depleted TANGO1L and TANGO1S and expressed TANGO1 SE and SA mutants. Immunofluorescence data are shown in Fig. 3E and quantitative data in Fig. 3F. Although wild-type TANGO1S and SA mutants efficiently rescued the dissociation between Sec16 and Sec31, SE mutants failed to correct the dissociation of ER exit sites. These data strongly suggest that CK1-mediated TANGO1 phosphorylation in PPS regulates ER exit site organization. We made series of mutations in the TANGO1 PPS to identify the critical residues for CK1 phosphorylation (Fig. S1C). We examined not only the binding properties between Sec16 and TANGO1 mutants (Fig. S1D), but also the organizing efficiency of TANGO1 mutants (Fig. S1E). The data indicated that the number of mutations affects both the binding properties and organization, while critical residues important for regulating ER exit site organization were not likely existed. Thus, the degree of phosphorylation in TANGO1's PPS by CK1 regulates the organization of ER exit sites.

CK1 is required for mitotic ER exit site dissociation

Because CK1δ and CK1ε are involved in various cellular functions ranging from circadian rhythm to cell cycle progression (Schittek and Sinnberg, 2014; Venerando et al., 2014), we next investigated the conditions under which CK1-mediated TANGO1 phosphorylation regulates ER exit site organization. Secretion from the ER is blocked during mitosis which dramatically affects ER exit site organization (Farmaki et al., 1999; Kreiner and Moore, 1990). However, the mechanisms of ER exit site dissociation during mitosis are unknown. Thus, we evaluated whether CK1-mediated ER exit site

dissociation is involved in this process. The cells were synchronized with double thymidine block, and metaphase cells were selected to analyze ER exit sites. As shown in Fig. 4A, Sec16 and Sec31 showed distinctive staining in metaphase, as previously reported (Hughes and Stephens, 2010). Quantitative analysis clearly indicated that colocalization coefficiency between Sec16 and Sec31 was significantly reduced during mitosis (Fig. 4B). Notably, reduced colocalization was also observed between TANGO1 and Sec31 in mitotic cells, suggesting that ER exit site dissociation occurs for both peripheral membrane proteins and membrane proteins (Fig. 4C and D). We next visualized the proteins at ER exit sites upon CK1 depletion during mitosis. Unexpectedly, cells synchronized at metaphase clearly showed punctate structures stained by both Sec16 and Sec31 (Fig. 4E). Quantitative analysis suggested that cells depleted of CK1 showed significantly increased colocalization coefficiency between Sec16 and Sec31 (Fig. 4F). Cells synchronized at prometaphase by nocodazole block also showed punctate structures visualized by detecting Sec16 and Sec31 upon CK1 knockdown (Fig. S2A and B). Moreover, colocalization between TANGO1 and Sec31 was also increased during mitosis upon CK1 depletion (Fig. 4G and H). These data suggest that CK1 is important for mitotic dissociation of the ER exit site. Next, we investigated whether phosphorylation of TANGO1 is involved in mitotic ER exit site dissociation. Phos-tag blot analysis of cells stably expressing TANGO1 constructs revealed that wild-type TANGO1 is hyperphosphorylated during mitosis (Fig. 4I). In contrast, TANGO1 SA mutants were not phosphorylated in mitotic cells, suggesting that mitotic TANGO1 phosphorylation predominantly occurs at the PPS (Fig. 4I). We then evaluated the effects of TANGO1 expression on ER exit site dissociation. As shown in Fig. 4J–M and Fig. S2C and D, the expression of TANGO1 SA mutants failed to dissociate ER exit sites during mitosis. These data strongly suggest that CK1 phosphorylates the TANGO1 PPS for ER exit site dissociation during mitosis.

In this study, we identified CK1 as a regulator of ER exit sites. CK1 overexpression dissociated the ER exit site. In contrast, CK1 depletion enlarged the ER exit sites. We found that CK1 phosphorylated the TANGO1 PPS, which reduced binding between TANGO1 and Sec16. We previously showed that TANGO1 and Sec16 organize ER exit sites through their interaction (Maeda et al., 2017). Interestingly, the interaction domain of TANGO1 to Sec16 is not on the PPS but rather on the Sec16-interacting region, a

domain approximately 40 amino acids downstream of the PPS. Structural analysis is necessary to determine how phosphorylation of PPS affects the binding between TANGO1 and Sec16. Cells depleted of CK1 showed enlarged ER exit sites, indicating that CK1-mediated TANGO1 phosphorylation occurs in interphase cells. CK1δ and CK1ε regulate the circadian rhythm (Yang et al., 2017). Thus, it would be interesting to evaluate whether phosphorylation of TANGO1 by CK1 regulates secretion from the ER in the circadian cycle. Future studies are needed to evaluate CK1-mediated regulation of ER exit site organization in interphase cells. Our results revealed that CK1 phosphorylates TANGO1, which is required for mitotic ER exit site dissociation. The scheme of ER exit site organization during the cell cycle is shown in Fig. 5. In interphase cells, TANGO1 interacts with Sec16 to recruit proteins to ER exit sites for efficient secretion. During mitosis, CK1 phosphorylates TANGO1 and the binding between TANGO1 and Sec16 are reduced, inducing ER exit site dissociation. At the end of mitosis, TANGO1 is likely dephosphorylated by an unidentified phosphatase and ER exit sites are reorganized. Cdc2-mediated p47 phosphorylation was reported to disorganize the ER exit site but how this signal regulates the ER exit site remains unknown (Kano et al., 2004). Studies of whether the signal affects CK1 activity should be conducted. Phosphatase activity may be regulated in a cell cycle-dependent manner. Indeed, several phosphatases have been reported to have reduced activity during mitosis (Nilsson, 2019). Studies are needed to clarify ER exit site organization during the cell cycle; however, this is the first report to describe the precise molecular mechanism of mitotic ER exit site dissociation.

MATERIALS AND METHODS

Antibodies

A female 6-wk-old Wistar rat (CLEA Japan) was immunized with FLAG-tagged Sec23A in TiterMax Gold (TiterMax USA). Splenocytes were fused with PAI mouse myeloma cells using polyethylene glycol (Roche). Hybridoma supernatants were screened by indirect ELISA with His-tagged Sec23A as the antigens. Positive hybridoma lines were subcloned, grown in serum-free medium (Nihon Pharmaceutical) supplemented with hypoxanthine-thymidine (Thermo Fisher Scientific), and purified with protein G-Sepharose (GE Healthcare; Saito et al., 2014). Polyclonal antibodies against Sec16-N (374–387 aa), Sec16-C (2,319–2,332 aa), and TANGO1-CT (1,884–1,898 aa for TANGO1L; 762–776 aa for TANGO1S) were raised in rabbits by immunization with keyhole limpet hemocyanin-conjugated peptides and affinity-purified by columns conjugated with the peptides (Thermo Fisher Scientific; Iinuma et al., 2007; Saito et al., 2009, 2011; Maeda et al., 2016; Tanabe et al., 2016). Polyclonal antibodies against Sec31 and TANGO1-CC1 were raised in rabbits by immunization with recombinant Sec31 (522-719 aa) or GST-tagged TANGO1L (1,231–1,340 aa) [TANGO1S (109–218 aa)] and affinity-purified by columns conjugated with GST-tagged Sec31 (522-719 aa) or ColdTF-tagged TANGO1 (1,231–1,340 aa [TANGO1S (109–218 aa)];Saito et al., 2011; Maeda et al., 2016; Tanabe et al., 2016). Other antibodies were as follows: CK1δ (rabbit; Proteintech), CK1ε (mouse; BD), GAPDH (mouse; Merck), FLAG (mouse; Merck), HA (rat; Roche), and Sec31 (mouse; BD).

Cell culture and transfection

HeLa and 293T cells were cultured in DMEM supplemented with 10% fetal bovine serum. Lipofectamine RNAi max (Thermo Fisher Scientific) was used for transfecting siRNA. For plasmids transfection, polyethylenimine “MAX” (polysciences) or Fugene 6 (Promega) were used. Doxycycline-inducible stable cell lines expressing TANGO1S-FLAG, TANGO1S (SA)-FLAG were made with lentivirus system described previously (Shin et al., 2006). Proteins were induced by incubation with 1 μg/ml doxycycline for the indicated times.

Double thymidine block

Cells treated with siRNAs were incubated for 22 h and then treated with 2.5 mM thymidine for 16 h. The cells were washed three times with PBS and released for 8 h. Then, the cells were incubated further with 2.5 mM thymidine for 16 h, washed three times with PBS and released for 10 h before fixation.

Nocodazole block

Cells treated with siRNA were incubated for 59 h and then treated with 100 ng/ml nocodazole for 13 h before fixation or collecting by shake-off.

Immunoprecipitation and western blotting

The experiments were essentially performed as described previously (Saito et al., 2014). Cells extracted with extraction buffer consisting of 20 mM Tris-HCl (pH7.4), 100 mM NaCl, 1 mM EDTA, 1% Triton X-100, and protease inhibitors were centrifuged at 20,000 g for 15 min at 4°C. Cell lysates were immunoprecipitated with FLAG M2 antibodies (SIGMA). The beads were washed with TBS/0.1% Triton X-100 for five times followed by elution with DYKDDDK peptide and processed for sample preparation.

Biotinylated Phos-tag detection

Biotinylated Phos-tag analysis of phosphorylated proteins were conducted essentially as described previously (Kinoshita et al., 2006). The samples were resolved by SDS-PAGE followed by blotting to PVDF membranes. The membranes were probed with Phos-tag Biotin (Fuji Film) and then probed with Streptavidin-conjugated HRP (Fuji Film) for detection.

siRNA oligos

Stealth select siRNAs for TANGO1S, TANGO1L, Sec23A, and Sec23B were purchased from Thermo Fisher Scientific. The oligo sequences used were
TANGO1S siRNA, 5'-GAAUUGUCGCUUGCGUUCAGCUGUU-3';
TANGO1L siRNA, 5'-CAACUCAGAGGAAAGUGAUAGUGUA-3';
Sec23A siRNA (1119), 5'-GGGUGAUUCUUUCAAUACUUCCUUA-3';
Sec23A siRNA (366), 5'-GCGUGGUCCUCAGAUGCCUUUGAUA-3';
Sec23B siRNA (1021), 5'-GCUGCAAAUGGUCACUGCAUUGAUA-3';
Sec23B siRNA (1923), 5'-CAGCAGCAUUCUAGCUGACAGAAUU-3'.

For control siRNA, Stealth RNAi™ siRNA negative control med GC (Thermo Fisher Scientific) was used.
Mission siRNA was purchased from Merck. The oligo sequences used were
CK1δ siRNA (707), 5'-CCAUCGAAGUGUUGUGUAA -3';
CK1δ siRNA (335), 5'-UGAUCAGUCGCAUCGAAUA-3';
CK1ε siRNA (149), 5'-ACAUCGAGAGCAAGUUCUA-3';
CK1ε siRNA (734), 5'-CCUCCGAAUUCUCAACAUA-3'.
For control siRNA, Mission siRNA Universal Negative Control #1 (Merck) was used.
The number in the parentheses represents the starting base pair of the target sequence.

Immunofluorescence microscopy

Immunofluorescence microscopy analysis was performed as described previously (Saito et al., 2014). Cells grown on coverslips were washed with PBS, fixed with methanol (6 min at −20°C), and then washed with PBS and blocked in blocking solution (5% BSA in PBS with 0.1% Triton X-100 for 30 min). After blocking, cells were stained with primary antibody (1 h at room temperature) followed by incubation with Alexa Fluor-conjugated secondary antibodies (Alexa Fluor 488, Alexa Fluor 568, and/or Alexa Fluor 647 for 1 h at room temperature). Images were acquired with confocal laser scanning microscopy (Plan Apochromat 63×/1.40 NA oil immersion objective lens; LSM 700; Carl Zeiss). The acquired images were processed with Zen 2009 software (Carl Zeiss). All imaging was performed at room temperature.

Quantification of Pearson's colocalization coefficient

HeLa cells were fixed and stained with indicated antibodies. Stained cells were analyzed by confocal laser scanning microscopy (Plan Apochromat 63×/1.40 NA oil immersion objective lens; LSM 700; Carl Zeiss) and processed with Zen 2011 software (Carl Zeiss). Intensity scanning and calculating coefficiency were performed by colocalization plugin Coloc2 in Fiji-ImageJ (Schindelin et al., 2012).

Quantification of ER exit site size

HeLa cells were fixed and stained with indicated antibodies. Stained cells were analyzed by confocal laser scanning microscopy (Plan Apochromat 63×/1.40 NA oil immersion

objective lens; LSM 700; Carl Zeiss) and processed with Zen 2011 software (Carl Zeiss). The size distribution of each ER exit site stained with Sec16 was analyzed by Fiji-ImageJ.

In vitro kinase assay

0.57 μM of purified recombinant GST-TANGO1 PPS+PRD-His_6 (1,651–1,907 aa for TANGO1L; 529–785 aa for TANGO1S) or GST-TANGO1 PPS+PRD (SA)-His_6 were incubated with 0.24 μM of CK1δ (1–317aa), 20 mM Tris-HCl (pH 7.4), 150 mM NaCl, 0.1% Triton X-100, 11.4 mM $MgCl_2$, and 5 mM [γ-^{32}P] ATP at 30 °C for 1h. Kinase assay was stopped by boiling with Laemmli Sample buffer. The samples were then subjected to SDS-PAGE followed by exposing with phosphor plate analyzed by Typhoon FLA9500 (GE healthcare).

Online supplemental material

Figure S1 shows the purity of recombinant proteins used in the *in vitro* kinase assay. Figure S2 shows the degree of phosphorylation in TANGO1 PPS and its correlation with the dissociation of ER exit sites. Figure S3 shows that CK1 is required for mitotic ER exit site dissociation according to nocodazole block analysis.

Acknowledgements

This work was supported by Grant-in-Aid for Scientific Research (18H06063 to M.M. and 17H03651 to K.S.) from the Ministry of Education, Culture, Sports, Science and Technology of Japan, by Takeda Science Foundation to K.S., The Uehara Memorial Foundation to K.S., and The Naito Foundation to K.S. and by Suzuken Memorial Foundation to M.M.

The authors declare no competing financial interests.

Author contributions: Miharu Maeda designed and performed research, analyzed data, and wrote the manuscript; Yukie Komatsu performed research; and Kota Saito designed and performed research, analyzed data, and wrote the manuscript.

REFERENCES

Bannykh, S.I., T. Rowe, and W.E. Balch. 1996. The organization of endoplasmic reticulum export complexes. *J Cell Biol*. 135:19-35.

Blom, N., S. Gammeltoft, and S. Brunak. 1999. Sequence and structure-based prediction of eukaryotic protein phosphorylation sites. *J Mol Biol*. 294:1351-1362.

Farmaki, T., S. Ponnambalam, A.R. Prescott, H. Clausen, B.L. Tang, W. Hong, and J.M. Lucocq. 1999. Forward and retrograde trafficking in mitotic animal cells. ER-Golgi transport arrest restricts protein export from the ER into COPII-coated structures. *J Cell Sci*. 112 (Pt 5):589-600.

Graves, P.R., and P.J. Roach. 1995. Role of COOH-terminal phosphorylation in the regulation of casein kinase I delta. *J Biol Chem*. 270:21689-21694.

Hornbeck, P.V., B. Zhang, B. Murray, J.M. Kornhauser, V. Latham, and E. Skrzypek. 2015. PhosphoSitePlus, 2014: mutations, PTMs and recalibrations. *Nucleic Acids Res*. 43:D512-520.

Hughes, H., and D.J. Stephens. 2010. Sec16A defines the site for vesicle budding from the endoplasmic reticulum on exit from mitosis. *J Cell Sci*. 123:4032-4038.

Kano, F., A.R. Tanaka, S. Yamauchi, H. Kondo, and M. Murata. 2004. Cdc2 kinase-dependent disassembly of endoplasmic reticulum (ER) exit sites inhibits ER-to-Golgi vesicular transport during mitosis. *Mol Biol Cell*. 15:4289-4298.

Kinoshita, E., E. Kinoshita-Kikuta, K. Takiyama, and T. Koike. 2006. Phosphate-binding tag, a new tool to visualize phosphorylated proteins. *Mol Cell Proteomics*. 5:749-757.

Kreiner, T., and H.P. Moore. 1990. Membrane traffic between secretory compartments is differentially affected during mitosis. *Cell Regul*. 1:415-424.

Lord, C., D. Bhandari, S. Menon, M. Ghassemian, D. Nycz, J. Hay, P. Ghosh, and S. Ferro-Novick. 2011. Sequential interactions with Sec23 control the direction of vesicle traffic. *Nature*. 473:181-186.

Maeda, M., T. Katada, and K. Saito. 2017. TANGO1 recruits Sec16 to coordinately organize ER exit sites for efficient secretion. *J Cell Biol*. 216:1731-1743.

Maeda, M., K. Saito, and T. Katada. 2016. Distinct isoform-specific complexes of TANGO1 cooperatively facilitate collagen secretion from the endoplasmic reticulum. *Mol Biol Cell*. 27:2688-2696.

Mashhoon, N., A.J. DeMaggio, V. Tereshko, S.C. Bergmeier, M. Egli, M.F. Hoekstra, and J. Kuret. 2000. Crystal structure of a conformation-selective casein kinase-1 inhibitor. *J Biol Chem*. 275:20052-20060.

Miller, E.A., and R. Schekman. 2013. COPII - a flexible vesicle formation system. *Curr Opin Cell Biol*.

Nilsson, J. 2019. Protein phosphatases in the regulation of mitosis. *J Cell Biol*. 218:395-409.

Pecot, M.Y., and V. Malhotra. 2004. Golgi membranes remain segregated from the endoplasmic reticulum during mitosis in mammalian cells. *Cell*. 116:99-107.

Saito, K., M. Chen, F. Bard, S. Chen, H. Zhou, D. Woodley, R. Polischuk, R. Schekman, and V. Malhotra. 2009. TANGO1 facilitates cargo loading at endoplasmic reticulum exit sites. *Cell*. 136:891-902.

Saito, K., M. Maeda, and T. Katada. 2017. Regulation of the Sar1 GTPase Cycle Is Necessary for Large Cargo Secretion from the Endoplasmic Reticulum. *Front Cell Dev Biol*. 5:75.

Saito, K., K. Yamashiro, N. Shimazu, T. Tanabe, K. Kontani, and T. Katada. 2014. Concentration of Sec12 at ER exit sites via interaction with cTAGE5 is required for collagen export. *J Cell Biol*. 206:751-762.

Santos, A.J., C. Nogueira, M. Ortega-Bellido, and V. Malhotra. 2016. TANGO1 and Mia2/cTAGE5 (TALI) cooperate to export bulky pre-chylomicrons/VLDLs from the endoplasmic reticulum. *J Cell Biol*. 213:343-354.

Schindelin, J., I. Arganda-Carreras, E. Frise, V. Kaynig, M. Longair, T. Pietzsch, S. Preibisch, C. Rueden, S. Saalfeld, B. Schmid, J.Y. Tinevez, D.J. White, V. Hartenstein, K. Eliceiri, P. Tomancak, and A. Cardona. 2012. Fiji: an open-source platform for biological-image analysis. *Nat Methods*. 9:676-682.

Schittek, B., and T. Sinnberg. 2014. Biological functions of casein kinase 1 isoforms and putative roles in tumorigenesis. *Mol Cancer*. 13:231.

Sengupta, P., P. Satpute-Krishnan, A.Y. Seo, D.T. Burnette, G.H. Patterson, and J. Lippincott-Schwartz. 2015. ER trapping reveals Golgi enzymes continually revisit the ER through a recycling pathway that controls Golgi organization. *Proc Natl Acad Sci U S A*. 112:E6752-6761.

Shin, K.J., E.A. Wall, J.R. Zavzavadjian, L.A. Santat, J. Liu, J.I. Hwang, R. Rebres, T. Roach, W. Seaman, M.I. Simon, and I.D. Fraser. 2006. A single lentiviral vector

platform for microRNA-based conditional RNA interference and coordinated transgene expression. *Proc Natl Acad Sci U S A*. 103:13759-13764.

Venerando, A., M. Ruzzene, and L.A. Pinna. 2014. Casein kinase: the triple meaning of a misnomer. *Biochem J*. 460:141-156.

Villeneuve, J., J. Duran, M. Scarpa, L. Bassaganyas, J. Van Galen, and V. Malhotra. 2017. Golgi enzymes do not cycle through the endoplasmic reticulum during protein secretion or mitosis. *Mol Biol Cell*. 28:141-151.

Warren, G., C. Featherstone, G. Griffiths, and B. Burke. 1983. Newly synthesized G protein of vesicular stomatitis virus is not transported to the cell surface during mitosis. *J Cell Biol*. 97:1623-1628.

Yang, Y., T. Xu, Y. Zhang, and X. Qin. 2017. Molecular basis for the regulation of the circadian clock kinases CK1δ and CK1ε. *Cell Signal*. 31:58-65.

Zaal, K.J., C.L. Smith, R.S. Polishchuk, N. Altan, N.B. Cole, J. Ellenberg, K. Hirschberg, J.F. Presley, T.H. Roberts, E. Siggia, R.D. Phair, and J. Lippincott-Schwartz. 1999. Golgi membranes are absorbed into and reemerge from the ER during mitosis. *Cell*. 99:589-601.

Zeuschner, D., W.J. Geerts, E. van Donselaar, B.M. Humbel, J.W. Slot, A.J. Koster, and J. Klumperman. 2006. Immuno-electron tomography of ER exit sites reveals the existence of free COPII-coated transport carriers. *Nat Cell Biol*. 8:377-383.

FIGURE LEGENDS

Figure 1. CK1 regulates ER exit site organization. (A) HeLa cells transfected with HA-CK1α, HA-CK1δ, or HA–CK1δ K38R were fixed and stained with anti-Sec16-C, anti-Sec31 (m), and anti-HA antibodies. Bars = 10 μm. (right) Magnification of the indicated regions on the left. Bars = 5 μm. (B) Quantification of Pearson's colocalization coefficient of (A). Error bars represent the mean ± SEM. *$p < 0.05$, n.s.: not significant. (C) 293T cells transfected with indicated constructs were lysed and the lysates were subjected to SDS-PAGE followed by western blotting with anti-HA, anti-CK1ε, anti-GAPDH, anti-TANGO1-CC1, anti-Sec16-N, and anti-Sec31 (r) antibodies. (D) HeLa cells transfected with the indicated siRNAs were fixed and stained with anti-Sec16-C, anti-Sec31(m) and anti-Sec23 antibodies. Bars = 10 μm. (E) Quantification of ER exit site size distribution of (D). (F) HeLa cells transfected with indicated siRNAs were lysed and the lysates were subjected to SDS-PAGE followed by western blotting with anti-CK1δ, anti-CK1ε, anti-GAPDH, anti-TANGO1-CC1, anti-Sec16-N, and anti-Sec31(r) antibodies. (G) HeLa cells were treated with either DMSO or 10 μM of IC261 for 12 h. Cells were fixed and stained with anti-Sec16-C, anti-Sec31(m), and anti-Sec23 antibodies. Bars = 10 μm. (H) Quantification of ER exit site size distribution of (G). (I) HeLa cells transfected with indicated siRNAs were treated with either DMSO or 10 μM of IC261 for 12 h. Cells were fixed and stained with anti-Sec16-C and anti-Sec23 antibodies. Bars = 10 μm. (J) Quantification of ER exit site size distribution of (I).

Figure 2. CK1 interaction reduces the binding affinity of Sec16 to TANGO1. (A) 293T cells were transfected with HA-CK1δ or HA-CK1δ K38R with FLAG-Sec16 constructs as indicated. Cell lysates were immunoprecipitated with anti-FLAG antibody and eluted with a FLAG peptide. Eluates were then subjected to SDS-PAGE followed by western blotting with anti-FLAG and anti-HA antibodies. (B) Schematic representation of human Sec16 domain organization. ELD, ER exit site localization domain; CCD, central conserved domain; CTCD, C-terminal conserved domain. (C) 293T cells were transfected with indicated FLAG-tagged Sec16 deletion constructs with HA-CK1δ constructs as indicated. Cell lysates were immunoprecipitated with anti-FLAG antibody and eluted with a FLAG peptide. Eluates were then subjected to SDS-PAGE followed by western blotting with anti-FLAG and anti-HA antibodies. (D) 293T cells were transfected with FLAG-Sec16 (1101–1890 aa) or TANGO1S-FLAG and HA-CK1δ or HA-CK1δ

K38R constructs. Cell lysates were immunoprecipitated with anti-FLAG antibody and eluted with a FLAG peptide. Eluates were then subjected to SDS-PAGE followed by western blotting with anti-FLAG and anti-HA antibodies. (E) 293T cells were transfected with FLAG-Sec16 (1101–1890 aa), TANGO1S-HA, and HA-CK1δ constructs as indicated. Cell lysates were immunoprecipitated with anti-FLAG antibody and eluted with a FLAG peptide. Eluates were then subjected to SDS-PAGE followed by western blotting with anti-FLAG and anti-HA antibodies.

Figure 3. CK1-mediated TANGO1 phosphorylation dissociates ER exit sites. (A) Schematic representation of TANGO1 domain organization. PPS, phosphorylation predicted sequences; SIR, Sec16-interacting region; PRD, proline-rich domain. (B) *In vitro* kinase assay was performed with purified recombinant GST-TANGO1 PPS+PRD-His_6 or GST-TANGO1 PPS+PRD (SA)-His_6 with CK1δ (1–317 aa). (C) 293T cells were transfected with FLAG-Sec16 and TANGO1S-HA or TANGO1S (SE)-HA or TANGO1S (SA)-HA constructs. Cell lysates were immunoprecipitated with anti-FLAG antibody and eluted with a FLAG peptide. Eluates were then subjected to SDS-PAGE followed by western blotting with anti-FLAG and anti-HA antibodies. (D) 293T cells were transfected with FLAG-Sec16 (1101–1890 aa), TANGO1S (SA)-HA, and HA-CK1δ constructs as indicated. Cell lysates were immunoprecipitated with anti-FLAG antibody and eluted with a FLAG peptide. Eluates were then subjected to SDS-PAGE followed by western blotting with anti-FLAG and anti-HA antibodies. (E) HeLa cells were treated with TANGO1L and TANGO1S siRNAs. After 24 h, indicated HA-tagged TANGO1S constructs were transfected and further cultured for 24 h. The cells were fixed and stained with anti-Sec16, anti-Sec31, and anti-HA antibodies. Bars = 10 μm. (F) Quantification of Pearson's colocalization coefficient of (E). Error bars represent means ± SEM. *$p < 0.05$, n.s.: not significant.

Figure 4. CK1 is required for mitotic ER exit site dissociation. (A) Non-treated HeLa cells and HeLa cells synchronized at mitotic phase with double thymidine block were fixed and stained with anti-Sec16-C, anti-Sec31(m), or TO-PRO3. (B) Quantification of Pearson's colocalization coefficient of (A). (C) Non-treated HeLa cells and HeLa cells synchronized at mitotic phase with double thymidine block were fixed and stained with anti-TANGO1-CT, anti-Sec31(m), or TO-PRO3. (D) Quantification of Pearson's

colocalization coefficient of (C). (E) HeLa cells transfected with indicated siRNAs were synchronized at mitotic phase with double thymidine block. Cells were then fixed and stained with anti-Sec16-C, anti-Sec31(m), or TO-PRO3. (F) Quantification of Pearson's colocalization coefficient of (E). (G) HeLa cells transfected with indicated siRNAs were synchronized at mitotic phase with double thymidine block. Cells were then fixed and stained with anti-TANGO1-CT, anti-Sec31(m), or TO-PRO3. (H) Quantification of Pearson's colocalization coefficient of (G). (I) Interphase extracts of doxycycline-inducible HeLa cells expressing either TANGO1S-FLAG or TANGO1S (SA)-FLAG were collected. Mitotic extracts were collected by treatment of nocodazole followed by shake-off. Cell lysates were immunoprecipitated with anti-FLAG antibody and eluted with a FLAG peptide. Eluates were subjected to SDS-PAGE followed by biotinylated Phos-tag detection or western blotting with anti-FLAG antibody. Lysates were subjected to SDS-PAGE followed by western blotting with anti-CK1δ, anti-GAPDH, and anti-cyclinB1 antibodies. (J) Doxycycline-inducible HeLa cells expressing either TANGO1S-FLAG or TANGO1S (SA)-FLAG were synchronized in the mitotic phase by double thymidine block. Cells were then fixed and stained with anti-Sec16-C, anti-Sec31(m), or TO-PRO3. (K) Quantification of Pearson's colocalization coefficient of (J). (L) Doxycycline-inducible HeLa cells expressing either TANGO1S-FLAG or TANGO1S (SA)-FLAG were synchronized in the mitotic phase by double thymidine block. Cells were then fixed and stained with anti-FLAG, anti-Sec31 (m), TO-PRO3. (M) Quantification of Pearson's colocalization coefficient of (L). Bars = 10 μm. Error bars represent the means ± SEM. *$p < 0.05$, n.s.: not significant.

Figure 5. Schematic diagram of mitotic ER exit site dissociation. In interphase cells, TANGO1 and Sec16 organize ER exit site. During mitosis, phosphorylation of TANGO1 by CK1 reduces its binding activity to Sec16 for ER exit site dissociation. At the end of mitosis, TANGO1 is dephosphorylated to reorganize ER exit site for secretion.

Figure S1. Degree of phosphorylation in TANGO1 PPS is correlated with ER exit site dissociation. (A) Alignment of human TANGO1 PPS with corresponding regions from other species. Identical amino acids are shaded in black, and similar amino acids are shaded in gray. (B) Recombinant proteins used in the *in vitro* kinase assay. Recombinant GST-TANGO1 PRD-His_6, GST-TANGO1 PRD (SA)-His_6, CK1δ (1–317 aa), and CK1δ

KR (1–317 aa) were resolved by SDS-PAGE followed by Coomassie brilliant blue staining. The asterisks indicate bacterial protein contaminants. (C) Sequences of human TANGO1 PPS mutants. (D) 293T cells were transfected with FLAG-Sec16 and indicated TANGO1S-HA mutants. Cell lysates were immunoprecipitated with anti-FLAG antibody and eluted with a FLAG peptide. Eluates were then subjected to SDS-PAGE followed by western blotting with anti-FLAG and anti-HA antibodies. (E) HeLa cells were treated with TANGO1L and TANGO1S siRNAs. After 24 h, indicated TANGO1S-HA mutants were transfected and further cultured for 24 h. The cells were fixed and stained with anti-Sec16-C, anti-Sec31(m) antibodies and quantified for Pearson's colocalization coefficient. Error bars represent the means ± SEM. *$p < 0.05$ compared to TANGO1LS KD, n.s.: not significant compared to TANGO1LS KD.

Figure S2. CK1 is required for ER exit site dissociation at prometaphase. (A) HeLa cells transfected with indicated siRNAs were synchronized in the mitotic phase by nocodazole block. Cells were then fixed and stained with anti-Sec16-C, anti-Sec31(m), and TO-PRO3. (B) Quantification of Pearson's colocalization coefficient of (A). (C) HeLa cells either non-treated or transfected with TANGO1S (SA)-HA were synchronized in the mitotic phase by nocodazole block. Cells were then fixed and stained with anti-Sec16-C, anti-Sec31(m), and anti-HA antibodies. (D) Quantification of Pearson's colocalization coefficient of (C). Bars = 10 μm. Error bars represent the means ± SEM. *$p < 0.05$.

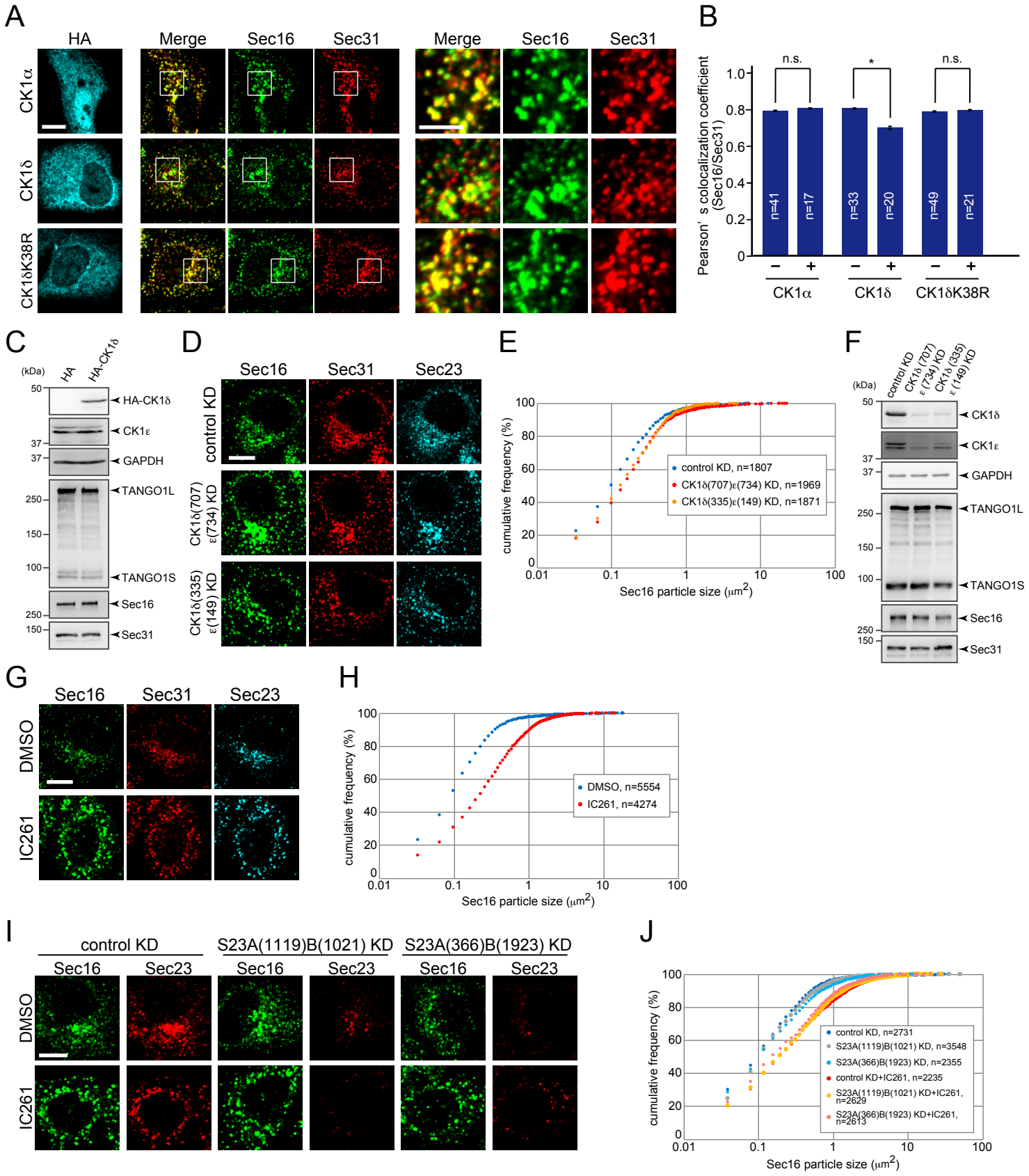
A
HA
Merge
Sec16
Sec31
Merge
Sec16
Sec31
CK1α
CK1δ
CK1δK38R
B
Pearson's colocalization coefficient (Sec16/Sec31)
n.s.
*
n.s.
n=41
n=17
n=33
n=20
n=49
n=21
CK1α
CK1δ
CK1δK38R
C
(kDa)
HA
HA-CK1δ
HA-CK1δ
CK1ε
GAPDH
TANGO1L
TANGO1S
Sec16
Sec31
D
Sec16
Sec31
Sec23
control KD
CK1δ(707) ε(734) KD
CK1δ(335) ε(149) KD
E
cumulative frequency (%)
Sec16 particle size (μm2)
control KD, n=1807
CK1δ(707)ε(734) KD, n=1969
CK1δ(335)ε(149) KD, n=1871
F
(kDa)
control KD
CK1δ (707) ε (734) KD
CK1δ (335) ε (149) KD
CK1δ
CK1ε
GAPDH
TANGO1L
TANGO1S
Sec16
Sec31
G
Sec16
Sec31
Sec23
DMSO
IC261
H
cumulative frequency (%)
Sec16 particle size (μm2)
DMSO, n=5554
IC261, n=4274
I
control KD
S23A(1119)B(1021) KD
S23A(366)B(1923) KD
Sec16
Sec23
Sec16
Sec23
Sec16
Sec23
DMSO
IC261
J
cumulative frequency (%)
Sec16 particle size (μm2)
control KD, n=2731
S23A(1119)B(1021) KD, n=3548
S23A(366)B(1923) KD, n=2355
control KD+IC261, n=2235
S23A(1119)B(1021) KD+IC261, n=2629
S23A(366)B(1923) KD+IC261, n=2613

Fig. 1

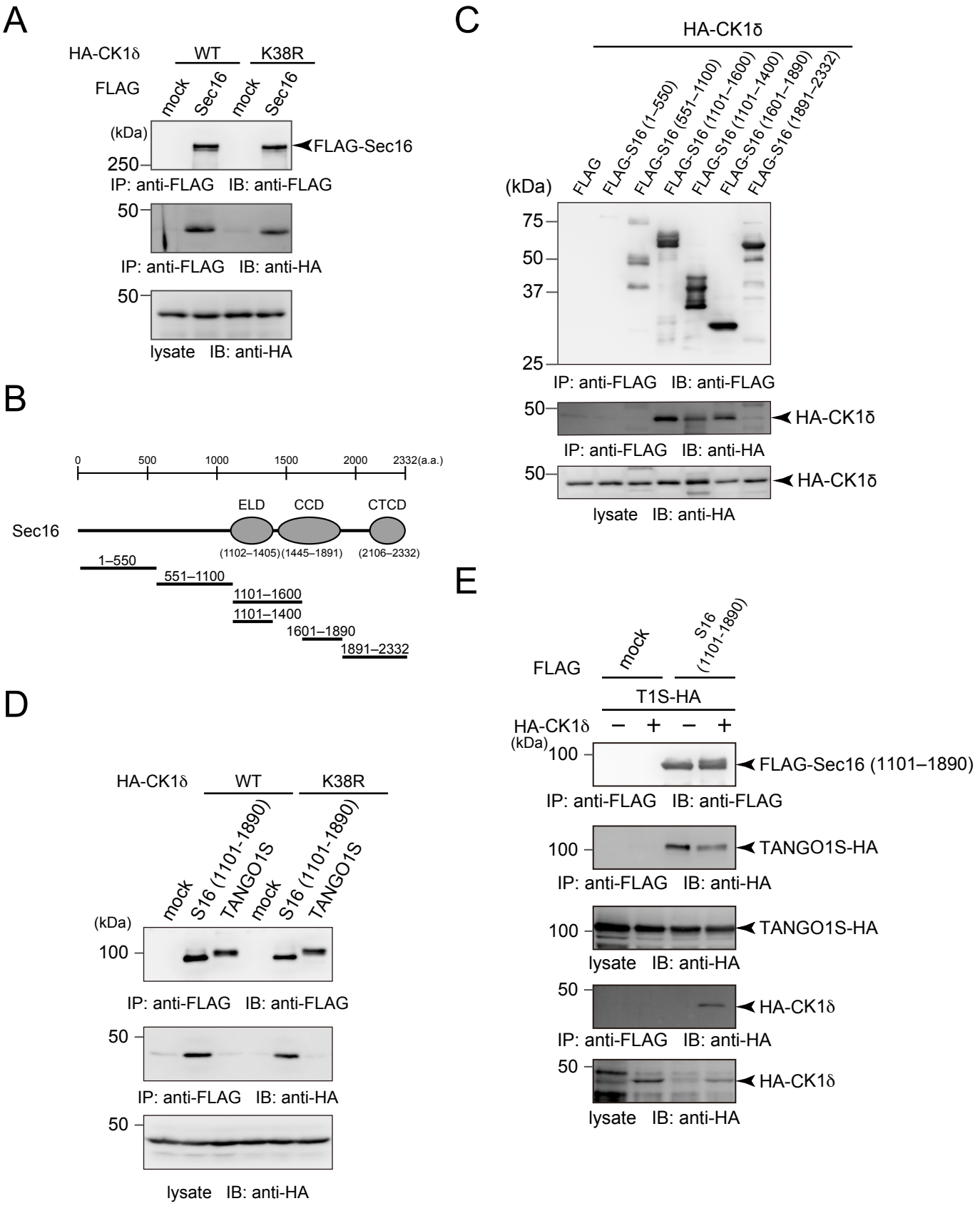
A
HA-CK1δ
WT
K38R
FLAG
mock
Sec16
mock
Sec16
(kDa)
250
FLAG-Sec16
IP: anti-FLAG IB: anti-FLAG
50
IP: anti-FLAG IB: anti-HA
50
lysate IB: anti-HA
B
0
500
1000
1500
2000
2332(a.a.)
Sec16
ELD
CCD
CTCD
(1102–1405)
(1445–1891)
(2106–2332)
1–550
551–1100
1101–1600
1101–1400
1601–1890
1891–2332
C
HA-CK1δ
FLAG
FLAG-S16 (1–550)
FLAG-S16 (551–1100)
FLAG-S16 (1101–1600)
FLAG-S16 (1101–1400)
FLAG-S16 (1601–1890)
FLAG-S16 (1891–2332)
(kDa)
75
50
37
25
IP: anti-FLAG IB: anti-FLAG
50
HA-CK1δ
IP: anti-FLAG IB: anti-HA
50
HA-CK1δ
lysate IB: anti-HA
D
HA-CK1δ
WT
K38R
mock
S16 (1101-1890)
TANGO1S
mock
S16 (1101-1890)
TANGO1S
(kDa)
100
IP: anti-FLAG IB: anti-FLAG
50
IP: anti-FLAG IB: anti-HA
50
lysate IB: anti-HA
E
FLAG
mock
S16 (1101-1890)
T1S-HA
HA-CK1δ
−
+
−
+
(kDa)
100
FLAG-Sec16 (1101–1890)
IP: anti-FLAG IB: anti-FLAG
100
TANGO1S-HA
IP: anti-FLAG IB: anti-HA
100
TANGO1S-HA
lysate IB: anti-HA
50
HA-CK1δ
IP: anti-FLAG IB: anti-HA
50
HA-CK1δ
lysate IB: anti-HA

Fig. 2

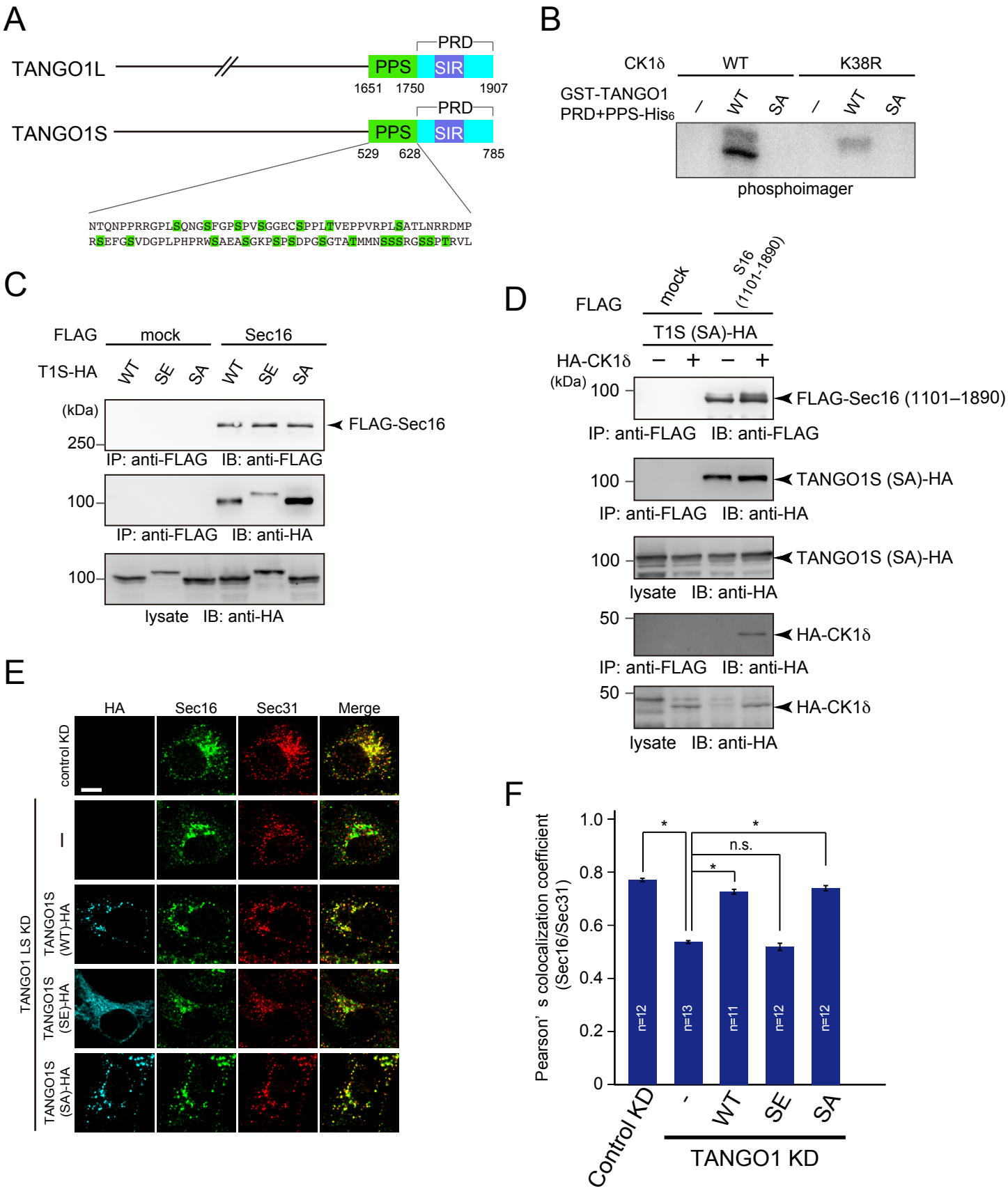
A
TANGO1L
PRD
PPS
SIR
1651
1750
1907
TANGO1S
PRD
PPS
SIR
529
628
785
NTQNPPRRGPLSQNGSFGPSPVSGGECSPPLTVEPPVRPLSATLNRRDMP
RSEFGSVDGPLPHPRWSAEASGKPSPSDPGSGTATMMNSSSRGSSPTRVL
B
CK1δ
WT
K38R
GST-TANGO1 PRD+PPS-His6
/
WT
SA
/
WT
SA
phosphoimager
C
FLAG
mock
Sec16
T1S-HA
WT
SE
SA
WT
SE
SA
(kDa)
250
FLAG-Sec16
IP: anti-FLAG IB: anti-FLAG
100
IP: anti-FLAG IB: anti-HA
100
lysate IB: anti-HA
D
FLAG
mock
S16 (1101-1890)
T1S (SA)-HA
HA-CK1δ
−
+
−
+
(kDa)
100
FLAG-Sec16 (1101–1890)
IP: anti-FLAG IB: anti-FLAG
100
TANGO1S (SA)-HA
IP: anti-FLAG IB: anti-HA
100
TANGO1S (SA)-HA
lysate IB: anti-HA
50
HA-CK1δ
IP: anti-FLAG IB: anti-HA
50
HA-CK1δ
lysate IB: anti-HA
E
HA
Sec16
Sec31
Merge
control KD
TANGO1 LS KD
-
TANGO1S (WT)-HA
TANGO1S (SE)-HA
TANGO1S (SA)-HA
F
Pearson' s colocalization coefficient (Sec16/Sec31)
1.0
0.8
0.6
0.4
0.2
0
*
*
n.s.
*
n=12
n=13
n=11
n=12
n=12
Control KD
-
WT
SE
SA
TANGO1 KD

Fig. 3

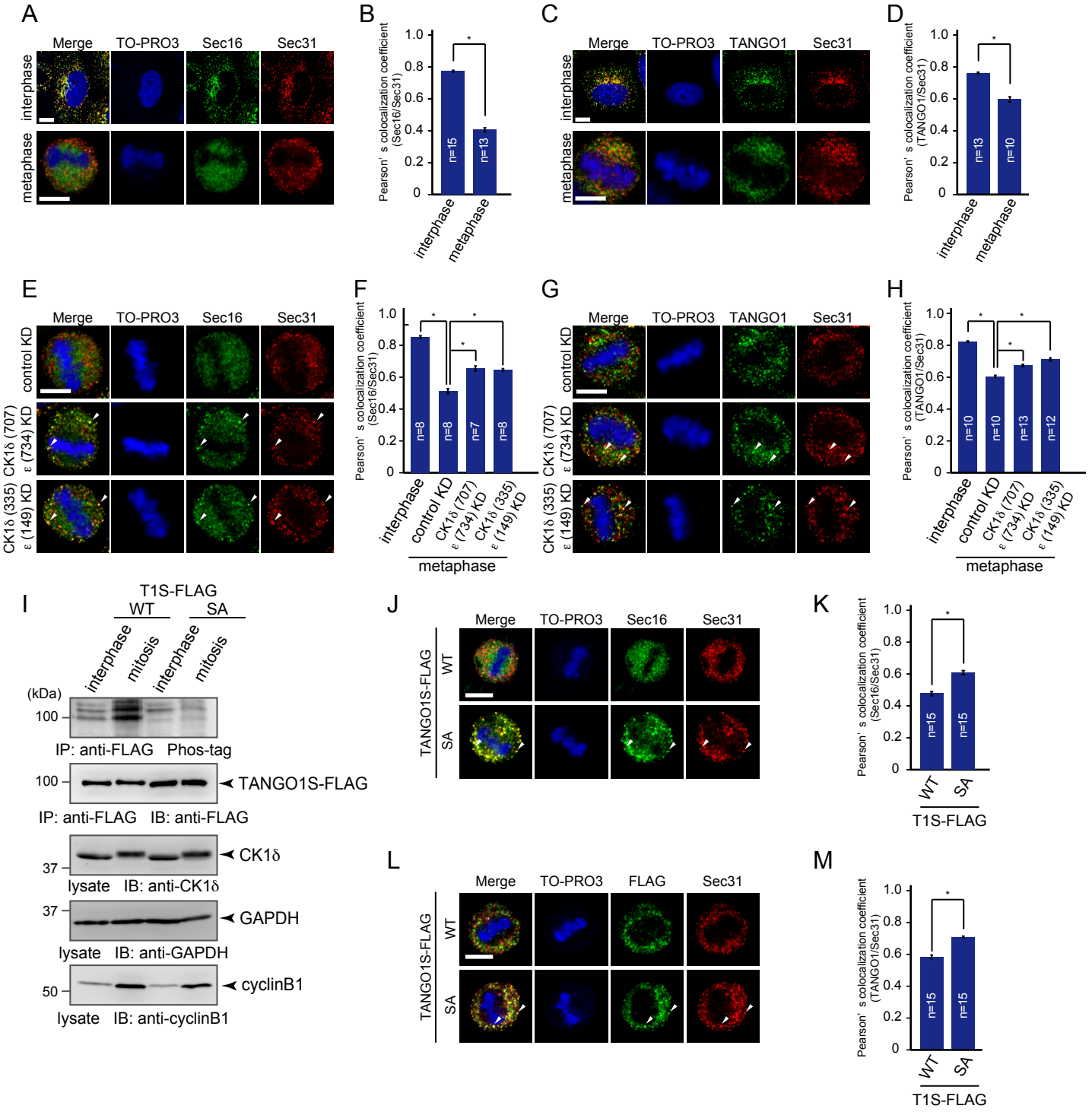
A
Merge
TO-PRO3
Sec16
Sec31
interphase
metaphase
B
Pearson' s colocalization coefficient (Sec16/Sec31)
n=15
n=13
interphase
metaphase
C
Merge
TO-PRO3
TANGO1
Sec31
interphase
metaphase
D
Pearson' s colocalization coefficient (TANGO1/Sec31)
n=13
n=10
interphase
metaphase
E
Merge
TO-PRO3
Sec16
Sec31
control KD
CK1δ (707) ε (734) KD
CK1δ (335) ε (149) KD
F
Pearson' s colocalization coefficient (Sec16/Sec31)
n=8
n=8
n=7
n=8
interphase
control KD
CK1δ (707) ε (734) KD
CK1δ (335) ε (149) KD
metaphase
G
Merge
TO-PRO3
TANGO1
Sec31
control KD
CK1δ (707) ε (734) KD
CK1δ (335) ε (149) KD
H
Pearson' s colocalization coefficient (TANGO1/Sec31)
n=10
n=10
n=13
n=12
interphase
control KD
CK1δ (707) ε (734) KD
CK1δ (335) ε (149) KD
metaphase
I
T1S-FLAG
WT
SA
interphase
mitosis
interphase
mitosis
(kDa)
100
IP: anti-FLAG
Phos-tag
100
TANGO1S-FLAG
IP: anti-FLAG
IB: anti-FLAG
37
CK1δ
lysate
IB: anti-CK1δ
37
GAPDH
lysate
IB: anti-GAPDH
50
cyclinB1
lysate
IB: anti-cyclinB1
J
Merge
TO-PRO3
Sec16
Sec31
TANGO1S-FLAG
WT
SA
K
Pearson' s colocalization coefficient (Sec16/Sec31)
n=15
n=15
WT
SA
T1S-FLAG
L
Merge
TO-PRO3
FLAG
Sec31
TANGO1S-FLAG
WT
SA
M
Pearson' s colocalization coefficient (TANGO1/Sec31)
n=15
n=15
WT
SA
T1S-FLAG

Fig. 4

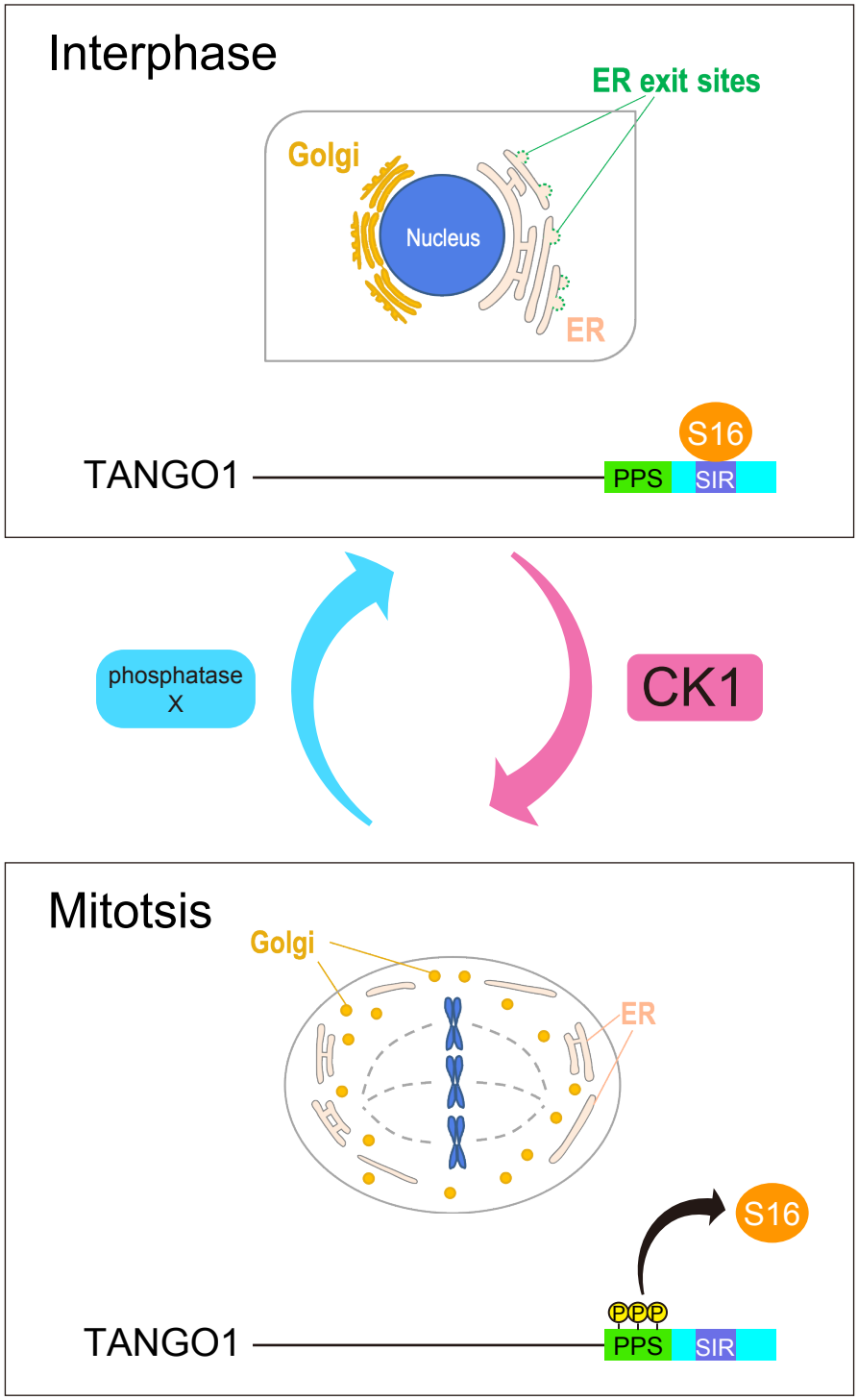
Interphase
ER exit sites
Golgi
Nucleus
ER
S16
TANGO1
PPS
SIR
phosphatase
X
CK1
Mitotsis
Golgi
ER
S16
PPP
TANGO1
PPS
SIR

Fig. 5

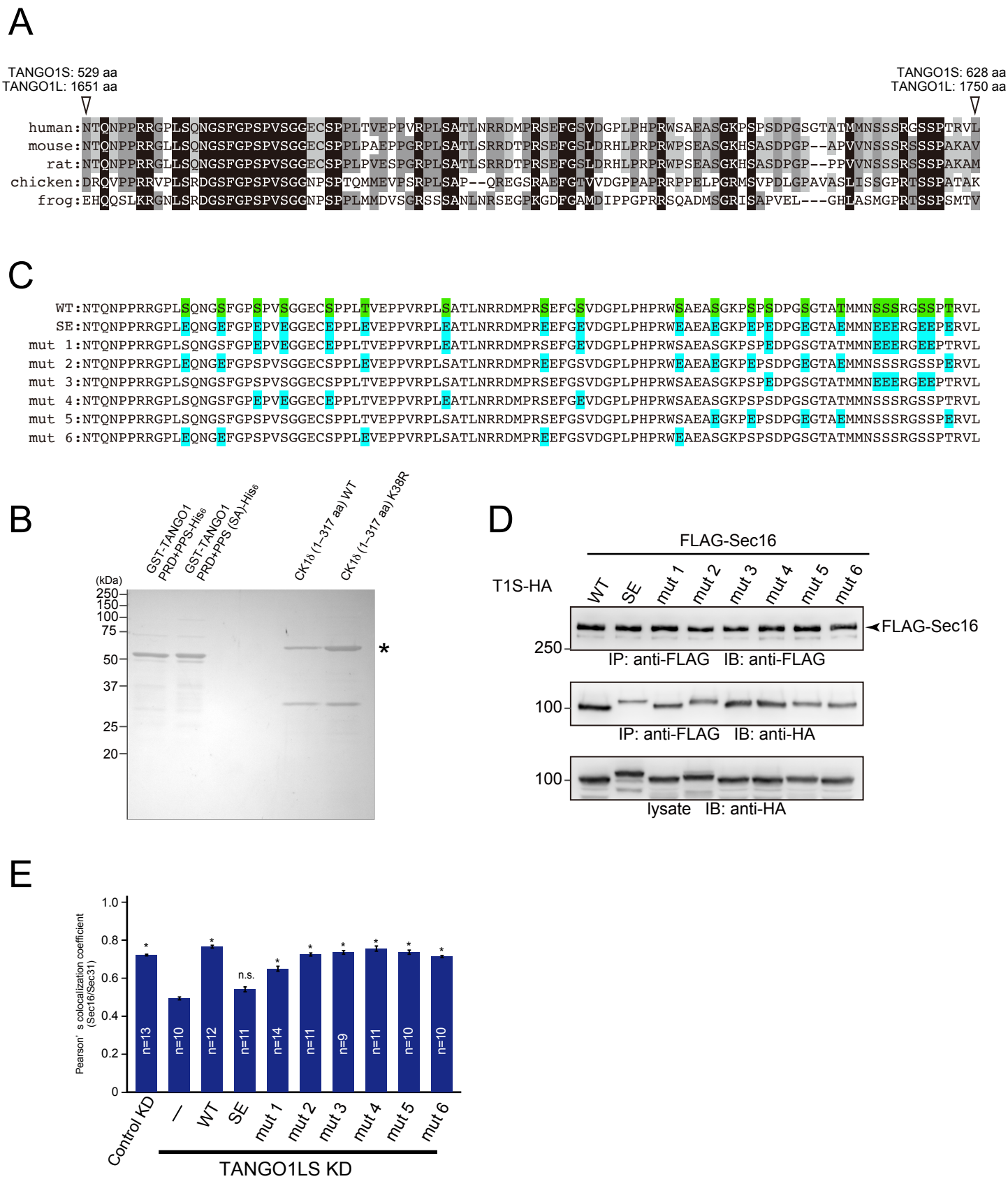
A
TANGO1S: 529 aa
TANGO1L: 1651 aa
TANGO1S: 628 aa
TANGO1L: 1750 aa
human:NTQNPPRRGPLSQNGSFGPSPVSGGECSPPLTVEPPVRPLSATLNRRDMPRSEFGSVDGPLPHPRWSAEASGKPSPSDPGSGTATMMNSSSRGSSPTRVL
mouse:NTQNPPRRGLLSQNGSFGPSPVSGGECSPPLPAEPPGRPLSATLSRRDTPRSEFGSLDRHLPRPRWPSEASGKHSASDPGP--APVVNSSSRSSSPAKAV
rat:NTQNPPRRGLLSQNGSFGPSPVSGGECSPPLPVESPGRPLSATLSRRDTPRSEFGSLDRHLPRPRWPSEASGKHSASDPGP--PPVVNSSSRSSSPAKAM
chicken:DRQVPPRRVPLSRDGSFGPSPVSGGNPSPTQMMEVPSRPLSAP--QREGSRAEFGTVVDGPPAPRRPPELPGRMSVPDLGPAVASLISSGPRTSSPATAK
frog:EHQQSLKRGNLSRDGSFGPSPVSGGNPSPPLMMDVSGRSSSANLNRSEGPKGDFGAMDIPPGPRRSQADMSGRISAPVEL---GHLASMGPRTSSPSMTV
C
WT:NTQNPPRRGPLSQNGSFGPSPVSGGECSPPLTVEPPVRPLSATLNRRDMPRSEFGSVDGPLPHPRWSAEASGKPSPSDPGSGTATMMNSSSRGSSPTRVL
SE:NTQNPPRRGPLEQNGEFGPEPVEGGECEPPLEVEPPVRPLEATLNRRDMPREEFGEVDGPLPHPRWEAEAEGKPEPEDPGEGTAEMMNEEERGEEPERVL
mut 1:NTQNPPRRGPLSQNGSFGPEPVEGGECEPPLTVEPPVRPLEATLNRRDMPRSEFGEVDGPLPHPRWSAEASGKPSPEDPGSGTATMMNEEERGEEPTRVL
mut 2:NTQNPPRRGPLEQNGEFGPSPVSGGECSPPLEVEPPVRPLSATLNRRDMPREEFGSVDGPLPHPRWEAEAEGKPEPSDPGEGTAEMMNSSSRGSSPERVL
mut 3:NTQNPPRRGPLSQNGSFGPSPVSGGECSPPLTVEPPVRPLSATLNRRDMPRSEFGSVDGPLPHPRWSAEASGKPSPEDPGSGTATMMNEEERGEEPTRVL
mut 4:NTQNPPRRGPLSQNGSFGPEPVEGGECEPPLTVEPPVRPLEATLNRRDMPRSEFGEVDGPLPHPRWSAEASGKPSPSDPGSGTATMMNSSSRGSSPTRVL
mut 5:NTQNPPRRGPLSQNGSFGPSPVSGGECSPPLTVEPPVRPLSATLNRRDMPRSEFGSVDGPLPHPRWSAEAEGKPEPSDPGEGTAEMMNSSSRGSSPERVL
mut 6:NTQNPPRRGPLEQNGEFGPSPVSGGECSPPLEVEPPVRPLSATLNRRDMPREEFGSVDGPLPHPRWEAEASGKPSPSDPGSGTATMMNSSSRGSSPTRVL
B
GST-TANGO1 PRD+PPS-His6
GST-TANGO1 PRD+PPS (SA)-His6
CK1δ (1–317 aa) WT
CK1δ (1–317 aa) K38R
(kDa)
250
150
100
75
50
37
25
20
*
D
FLAG-Sec16
T1S-HA
WT
SE
mut 1
mut 2
mut 3
mut 4
mut 5
mut 6
FLAG-Sec16
250
IP: anti-FLAG IB: anti-FLAG
100
IP: anti-FLAG IB: anti-HA
100
lysate IB: anti-HA
E
Pearson's colocalization coefficient (Sec16/Sec31)
1.0
0.8
0.6
0.4
0.2
0
n.s.
n=13
n=10
n=12
n=11
n=14
n=11
n=9
n=11
n=10
n=10
Control KD
—
WT
SE
mut 1
mut 2
mut 3
mut 4
mut 5
mut 6
TANGO1LS KD

Fig. S1

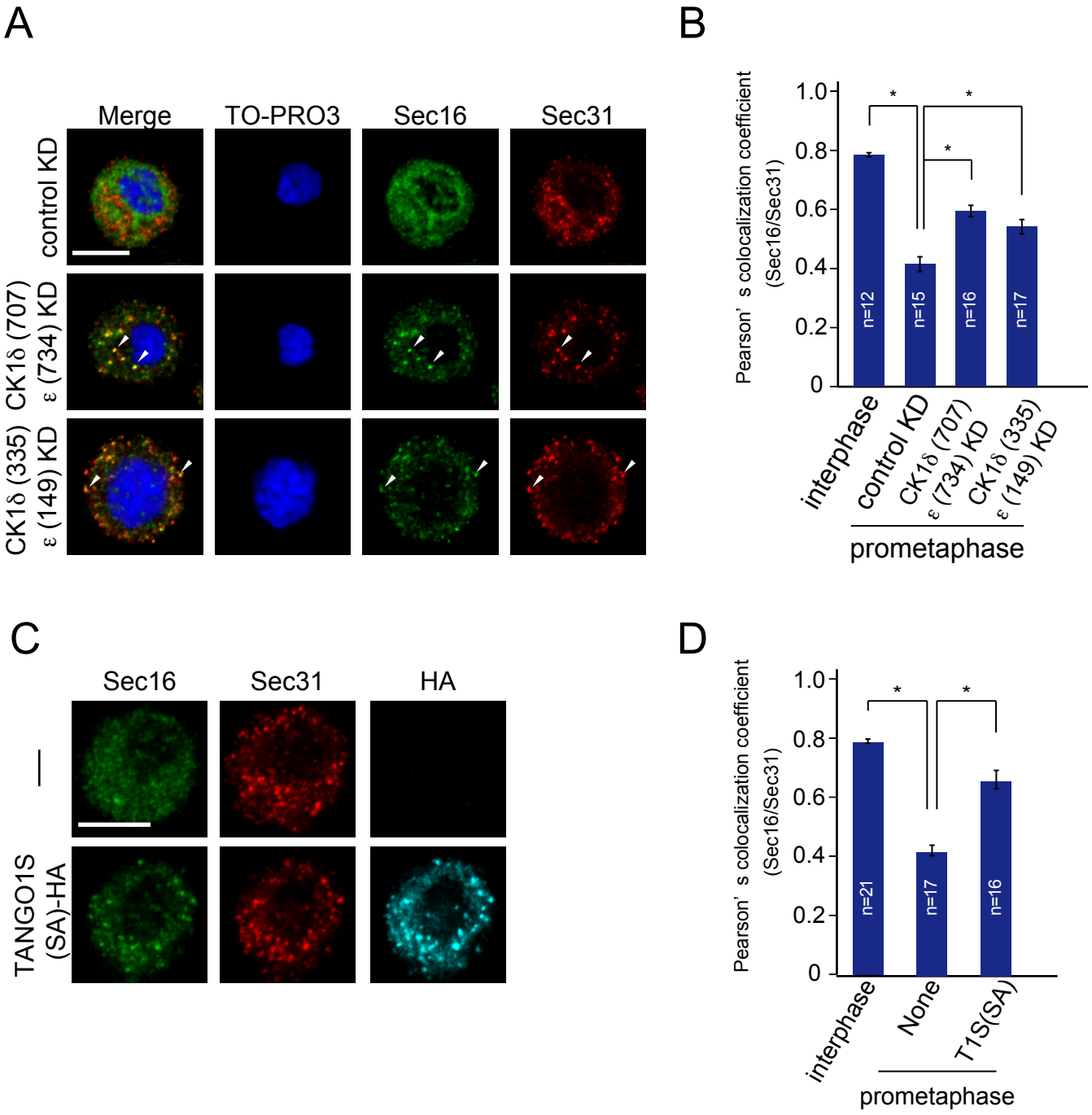
A
Merge
TO-PRO3
Sec16
Sec31
control KD
CK1δ (707) ε (734) KD
CK1δ (335) ε (149) KD
B
Pearson's colocalization coefficient (Sec16/Sec31)
1.0
0.8
0.6
0.4
0.2
0
*
*
*
n=12
n=15
n=16
n=17
interphase
control KD
CK1δ (707) ε (734) KD
CK1δ (335) ε (149) KD
prometaphase
C
Sec16
Sec31
HA
—
TANGO1S (SA)-HA
D
Pearson's colocalization coefficient (Sec16/Sec31)
1.0
0.8
0.6
0.4
0.2
0
*
*
n=21
n=17
n=16
interphase
None
T1S(SA)
prometaphase

Fig. S2